Title: Hydrogen Bonding of Ethanol in Supercritical Mixtures with CO_2 by ^{1}H NMR Spectroscopy and Molecular Simulation

Authors: Steffen Reiser, Nichola McCann, Martin Horsch, Hans Hasse

PII: S0896-8446(12)00155-6
DOI: doi:10.1016/j.supflu.2012.04.014
Reference: SUPFLU 2452

To appear in: *J. of Supercritical Fluids*

Received date: 15-3-2012
Revised date: 19-4-2012
Accepted date: 20-4-2012

Please cite this article as: S. Reiser, N. McCann, M. Horsch, H. Hasse, Hydrogen Bonding of Ethanol in Supercritical Mixtures with CO_2 by ^{1}H NMR Spectroscopy and Molecular Simulation, *The Journal of Supercritical Fluids* (2010), doi:10.1016/j.supflu.2012.04.014

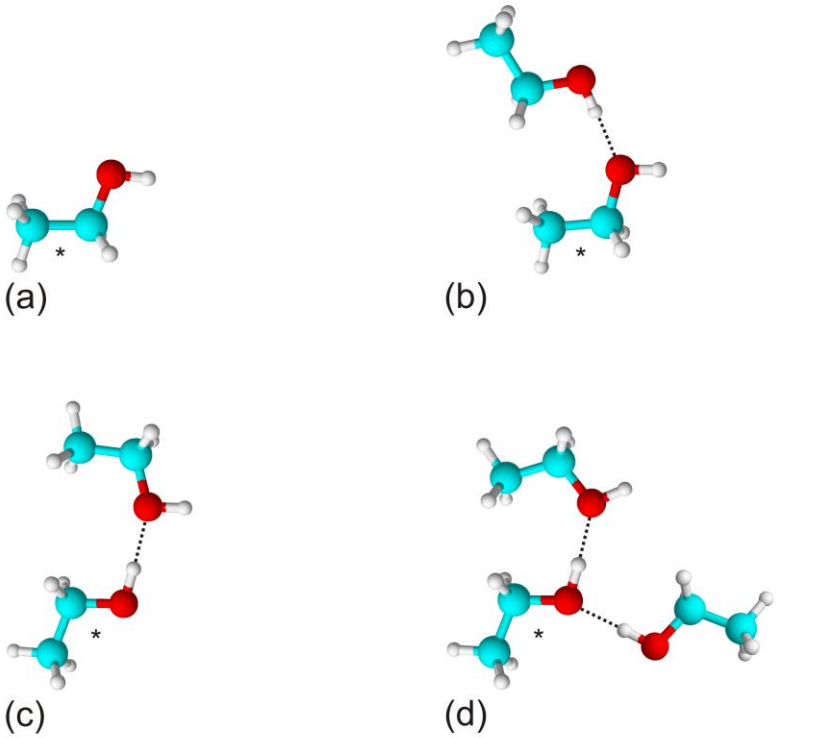

Highlights:

- ^{1}H NMR studies of supercritical CO_2-ethanol mixtures were conducted.
- MD with LJ plus point charges was used to describe hydrogen bonding in the mixture.
- Physico-chemical properties are well described by the model.

Hydrogen Bonding of Ethanol in Supercritical Mixtures with CO_2 by ^1H NMR Spectroscopy and Molecular Simulation

*Steffen Reiser, Nichola McCann, Martin Horsch, Hans Hasse**

Laboratory of Engineering Thermodynamics, University of Kaiserslautern, Germany

* Corresponding author. Address: Prof. Dr.-Ing. Hans Hasse, Laboratory of Engineering Thermodynamics, Department of Mechanical and Process Engineering, University of Kaiserslautern, Erwin-Schrödinger-Straße 44, 67663 Kaiserslautern, Germany.
Tel.: +49 (0)631 205 3464; Fax: +49 (0)631 205 3835. E-mail: hans.hasse@mv.uni-kl.de.

Abstract

High pressure ^1H NMR spectroscopic studies of mixtures of CO_2 and ethanol (EtOH) were conducted at a wide range of temperatures (293.15, 308.15, 323.15, and 338.15 K), pressures (5 - 25.5 MPa) and concentrations (x_{EtOH} = 0.0017 – 1.0 mol/mol). The relative chemical shift of the protons in the hydroxyl group was used to describe the degree of hydrogen bonding in ethanol. The dependence of the results on pressure is only weak. The quantification of hydrogen bonding was based on the assumption that the observed shift results from a superposition of the shifts of ethanol molecules differing in the way they are hydrogen bonded. Three different types were distinguished: monomer, donor and acceptor. The monomer shift was found from an extrapolation of the NMR data. Molecular dynamics simulations based on force fields from the literature were carried out for the same mixtures at

the same conditions and were used to determine the distribution of differently hydrogen bonded ethanol species. Geometric cluster criteria from the literature were used for identifying the hydrogen bonding and the different types of ethanol species. Using the species distribution from the molecular simulations together with the NMR spectroscopic data, the two state independent numbers for the shifts of the hydrogen bond donor and hydrogen bond acceptor molecules were found. Even though only these two parameters are fitted the large set of experimental data is very well described. This confirms our earlier observations on the CO_2-methanol system that molecular models of the simple Lennard-Jones plus point charge type as they are used here can describe both thermodynamic properties and the structural effects of hydrogen bonding in solutions.

Keywords

Hydrogen bonding, ethanol, molecular dynamics simulation, NMR spectroscopy.

1. Introduction

Hydrogen bonding has a remarkable effect on the properties of fluids. Consequently, it has been studied intensively for many decades now, both experimentally and using molecular simulations with quantum chemical and force field methods [1]. It is well known that NMR spectroscopy can be used for quantifying hydrogen bonding in solutions [2-6]. Our group recently published a study on hydrogen bonding in methanol mixtures with supercritical CO_2 in which a large body of experimental data was generated over a wide range of pressure and temperature conditions using high pressure online NMR spectroscopy [7]. The experimental results were compared to results from molecular simulations with force fields taken from the literature [8]. The methanol force field [8] consists of two united-atom Lennard-Jones (LJ) sites, accounting for dispersion and repulsion of the methylene and the hydroxyl group and three point charges located in the centers of the LJ sites and at the position of hydroxyl

hydrogen atom. The force field of CO_2 was also taken from previous work [9] and is of the two center LJ plus quadrupole type. The molecular models are known to accurately predict thermodynamic properties such as vapor pressure, saturated density, and enthalpy of vaporization [8, 9]. The study [8] shows that they are also successful in quantitatively predicting hydrogen bonding.

This cannot be expected a priori as hydrogen bonding is accounted for in the methanol force field only by partial charges and is, hence, lumped with polarity. Note that the same approach is taken in the vast majority of force fields for hydrogen bonding components. The results of Schnabel et al. [8] show that this simple approach also yields reasonable results for structural properties like hydrogen bonding. This approach is successful because appropriately placed interactions between partial charges give rise to interaction potentials which are directional and strongly attractive [10]. The determined potentials can even reflect stoichiometric properties in that a second partner is unable to bind to an already occupied site. Furthermore, polarity and hydrogen bonding can be separated using this approach. This is illustrated in Fig. 1, which shows two molecules modeled by a single LJ site with two point charges. Both molecules have the same dipole moment as calculated from the partial charge and the distance *a*. But they differ strongly in what is considered to be their ability to form hydrogen bonds, as determined by the charge and the distance, *b*, which is the distance from the position of the charge to the "border" of the Lennard-Jones sphere as determined by its diameter σ.

It is the aim of this study to extend our previous work on methanol to ethanol and hence to see whether the encouraging findings of the methanol study were a lucky coincidence or whether they have a more general background.

Numerous studies have been published on the hydrogen bonding in the CO_2-ethanol system [11-15]. Most recently, Xu and co-workers [11, 12] investigated the microscopic structure and hydrogen bonding statistics of ethanol in CO_2 under isobaric conditions using ab initio calculations and Monte Carlo simulations with force fields of the same type as discussed above. Equilibrium constants were determined to describe the size and relative amounts of hydrogen bonded aggregates as a function of temperature (323 - 343 K) and concentration (x_{EtOH} = 0.01 – 1 mol/mol). The molecular models of ethanol and CO_2 were validated against binary vapor-liquid equilibria data taken from the literature. The simulated results are in very good agreement with the experimental data.

Investigations into the dynamics of hydrogen bonding in CO_2-ethanol mixtures have revealed that hydrogen bonds between CO_2 and ethanol molecules are limited both in number and lifetime [13, 14]. This finding has been supported by Car-Parrinello molecular dynamics simulations which show that an electron donor-acceptor complex between CO_2 and ethanol is more stable than a hydrogen bonded complex of the two molecules [15].

In this work, we describe the generation of an extensive data set of ^{1}H NMR chemical shifts for the CO_2-ethanol system under a wide range of pressure (5 – 25.5 MPa), temperature (293.15 – 338.15 K) and composition (x_{EtOH} = 0.0017 – 1.0 mol/mol) conditions. Each NMR spectrum consists of three peaks, attributable to the OH, CH_2 and CH_3 moieties. The chemical shifts of all three peaks change with the variable conditions (concentration, temperature and pressure). The effect of these variables on the CH_2 and CH_3 shifts are the same, and can be attributed to non-hydrogen bonding effects. The shift of the OH peak, relative to the other two (δ_{CHn}) reflects purely hydrogen bonding effects.

Molecular dynamics simulations of mixtures with concentrations, temperatures, and pressures matching those defined in the experimental section were used to determine the hydrogen

bonding statistics of ethanol. From these simulations, the distribution of differently hydrogen bonded ethanol species was determined using geometric hydrogen bonding criteria. The characterization of the different species types and the geometric criteria is described in Section 3.3. The state independent chemical shift of the ethanol monomer was directly obtained from experimental data. The state independent chemical shifts of ethanol molecules acting as hydrogen bond acceptor and donor respectively were determined from a fit to the experimental data at 15 MPa. This fit was based on species distributions determined from molecular simulations and the corresponding contributions of each species to the relative chemical shift of the OH peak (δ_{CHn}) as described by Schnabel et al. [8]. As in the methanol investigation, [8] in this work, excellent agreement between the experimentally determined relative chemical shift and the predictions from molecular simulations was observed. This holds for the entire NMR spectroscopic data set and indicates that the simple LJ plus point charge molecular models are useful for describing not only thermodynamic properties of hydrogen bonding mixtures but also the structures formed as a result of hydrogen bonding.

2. Experimental

The apparatus used for sample preparation, circulation, temperature and pressure regulation has been described previously in detail [7] and is therefore presented here only briefly. A schematic of the set-up is shown in Fig 2. The cell consists of a high pressure cylinder with plunger allowing a volume change within the cell of approximately 90 %. The plunger, all valves (SLPV21 and SLPV23, Butech) and the lines to the NMR spectrometer are liquid thermostated. The cell is connected to a vacuum pump (Vacuubrand RZ 2.5) at V1. CO_2 and N_2 for purging are introduced to the cell via V6 and exhausted via V5. Liquid from the balance at C2 is introduced to the cell via V4. The line from V4 to C2 must be filled with

liquid prior to sample introduction. The sample is mixed via circulation through V8 using a gear pump (MCP-Z, Ismatec). The sample is transferred to the NMR spectrometer via V7. A 10 μm filter, F1 (A330, Upchurch) prevents any particulates from entering the capillary tubes. Before entering the NMR probe head, the flow is split, with the majority returning to the cell via a bypass and V4. The sample leaving the NMR probe head is transferred to a vibrating tube densimeter, D1 (DMA 512, Anton Paar) before being returned to the cell via V3. The temperature within the densimeter was not strictly regulated, and this property was measured for monitoring purposes only. Within this scope, measured values were in reasonable agreement with the literature and are not reported herein. A pressure meter, P1 (HKM-375M-350 bar, Kulite Semi Conductor Products) is mounted before the cell in the NMR return line. The pressure sensor was calibrated prior to measurement using a pressure balance (Desgranges & Huot, D+H Model 5201 "S") and is accurate to ±0.01 MPa. T1 is a temperature sensor with feedback to the thermostatting water bath. After each measurement, the sample is emptied from the cell via V5. A sapphire window at the front side of the cylinder (F) allows observation of the sample to regulate the phase behavior.

^{1}H NMR spectra were obtained on a Varian 400 MHz Unity Inova, using a supercritical fluid probe head from Bruker, as described previously [7]. The number of transients obtained ranged from 8 (pure ethanol) to 32, for the more dilute solutions. The measuring cell contains a concentric lock capillary along the high pressure sapphire cell for a reference solution. The temperature sensor within the NMR spectrometer is reportedly accurate to ±1 K and was calibrated using the temperature dependencies of the chemical shifts of ethylene glycol [16].

Spectroscopy grade ethanol (≥99.9%) was obtained from Merck and used without further purification. Liquid CO_2 was obtained from Air Liquide. The lock capillary was filled with approximately 10 % tetramethylsilane (TMS, ≥99.9%, Sigma Aldrich) in Acetone-d_6 (99.8%,

Deutero) as reference and lock solvent. Measurements were carried out at four temperatures: 293.15 K; 308.15 K; 323.15 K; and 338.15 K at pressures between 5 and 25.5 MPa. The ethanol mole fraction was varied within the range x_{EtOH} = 0.0017 – 1.0 mol/mol. Prior to each measurement, the apparatus was dried by a minimum of three vacuum-purge cycles at 338.15 K, using N_2 at >5 MPa as the purge gas, then evacuated.

The mass of ethanol used was determined from the mass difference at balance C2 (± 0.1 mg) before and after filling. The mass of CO_2 used was determined by the mass difference of the CO_2 pressure bomb before and after filling (± 1 mg). The CO_2 mass lost within the transfer line (between the pressure bomb and V6) was determined after measurement. The cell was mixed for at least 15 minutes prior to measurement. The sample was considered to be thoroughly mixed when repeat spectra taken at least 5 minutes apart showed no change in peak positions. After each change in pressure or temperature, equilibrium was assumed to have been reached once the pressure and density remained constant. This was verified by the measurement of at least two spectra taken at least five minutes apart with the same chemical shifts, within experimental error, for all peaks. The values reported are an average of these repeat measurements.

3. Molecular simulation

3.1. Molecular models

In this study, rigid, non-polarizable molecular models of the united-atom type were used. The molecular models for ethanol [17] and CO_2 [9] were taken from previous work of our group. Here, ethanol is composed of three LJ sites accounting for repulsion and dispersion of the methyl, methylene and hydroxyl groups. Point charges are located at the LJ centers of the methylene and hydroxyl group as well as at the hydroxyl hydrogen atom to model both

polarity and hydrogen bonding. The full description of the ethanol model is given by Fig. 3 and Table 1.

The molecular model of ethanol accurately describes thermodynamic properties such as vapor pressure, saturated density and enthalpy of vaporization [10, 17]. The force field of CO_2 is modeled as a symmetric two-center LJ plus point quadrupole. The interested reader is referred to the original publications [9, 17] for detailed information.

The potential energy between two molecules *i* and *j* of the same type is given by:

$$u_{ij}(r_{ijab}) = \sum_{a=1}^{n}\sum_{b=1}^{n} 4\varepsilon_{ab}\left[\left(\frac{\sigma_{ab}}{r_{ijab}}\right)^{12} - \left(\frac{\sigma_{ab}}{r_{ijab}}\right)^{6}\right] + \frac{q_{ia}q_{ib}}{4\pi\varepsilon_o r_{ijab}}, \quad (1)$$

where *n* is the number of sites in the molecular model, *a* the site index of molecule *i* and *b* the site index of molecule *j*. r_{ijab} represents the site-site distance between molecules *i* and *j*. σ_{ab} and ε_{ab} are the LJ size and energy parameters. The point charges located at the sites *a* and *b* of the molecules *i* and *j* are denoted by q_{ia} and q_{jb}, respectively, and ε_0 is the vacuum permittivity.

In order to define a molecular model which describes binary mixtures on the basis of pairwise additive pure substance models, only the unlike interactions between molecules must be defined. In mixtures of polar molecules, the electrostatic contribution of the unlike interaction is fully determined by the laws of electrostatic interactions. For the unlike LJ parameters, the modified Lorenz-Berthelot [18, 19] combining rules were employed:

$$\sigma_{ab} = \frac{\sigma_{aa} + \sigma_{bb}}{2} \quad (2)$$

$$\varepsilon_{ab} = \xi\sqrt{\varepsilon_{aa}\varepsilon_{bb}} \quad (3)$$

The binary interaction parameter ξ was fitted to the experimentally determined Henry's law constant at 298.15 K [17, 20] to give ξ = 0.992. Fig. 4 shows the vapor-liquid equilibrium simulation results [17, 20] at 323.15 K as well as the simulated density at the same temperature at 15 MPa, both with ξ = 0.992, in comparison to experimental data [21-24]. The simulation results both for the vapor-liquid equilibrium and the density compare favorably with the experimental results.

3.2. Simulation details

The distribution of the differently hydrogen bonded ethanol species was calculated from isobaric-isothermal (*NpT*) ensemble molecular dynamics simulations. The simulations were conducted to replicate the conditions used in the experimental section. In addition, simulations of mixtures with x_{EtOH} = 0.1, 0.2, 0.4, 0.6 and 0.8 mol/mol at 15 MPa were performed. The minimum number of molecules in the system was set to 864. In order to obtain meaningful hydrogen bonding statistics, simulations were performed with at least 54 ethanol molecules present in the simulation box with periodic boundary conditions. As a result, at low mole fractions of ethanol, the number of molecules increased up to 32,000, so a combination of Verlet [25] and cell lists [26, 27] was used. The molecular dynamics simulations were performed using the leapfrog integrator [28] with a time step of 1.5 fs. The simulations were equilibrated over 250,000 time steps followed by a production run over 200,000 time steps. The cut-off radius was set to 10 Å and the coulombic interactions were corrected using the reaction field method [28].

3.3. Hydrogen bonding criteria

A simple yet robust set of geometric criteria for hydrogen bonding of ethanol has been introduced by Saiz et al. [29]. According to these criteria, two ethanol molecules are considered to be hydrogen bonded if their oxygen site-site separation distance (r_{OO}) is below

3.5 Å, the hydrogen site to oxygen site separation distance (r_{OH}) is below 2.6 Å, and the angle between oxygen-oxygen alignment and the oxygen-hydrogen bond ($\theta_{O\cdots OH}$) is less than 30°. These criteria were derived from the radial distribution functions of pure liquid ethanol obtained from molecular dynamics simulations and validated against experimental X-ray scatter data. The same geometric criteria have been suggested based on structural information obtained from pair distribution functions determined from Monte Carlo simulations [12]. Recently, Skarmoutsos and Guardia [13] showed that these criteria are also valid for high pressure conditions. Interestingly, these geometric criteria for hydrogen bonds are identical to the hydrogen bonding criteria in other liquid alcohols [30] such as methanol [31]. They have been successfully used in previous studies to identify hydrogen bonds in methanol [32-34] and ethanol [14, 34-36] systems. We have previously used these criteria to successfully predict hydrogen bonding properties of methanol under a wide range of conditions [8].

In this work, application of the above-mentioned criteria resulted in the identification of hydrogen bonded species with i = 0, 1, 2 or 3 hydrogen bonds per molecule. The species fraction f_i is the number of ethanol molecules with i hydrogen bonds divided by the total number of ethanol molecules. Fig. 5 shows some important configurations of hydrogen-bonded ethanol molecules. f_0 represents ethanol monomers without hydrogen bonds, see Fig. 5 (a). Molecules in dimers (see Fig. 5 (b)) and at the end of hydrogen bonded chains (Fig. 5 (c)) are classified as f_1. In contrast, ethanol molecules that are within a hydrogen bonded chain, such as the central molecule of a trimer (see Fig. 5 (d) and (e)) contribute to f_2. The central molecule in cross-linked chains contributes to f_3.

4. Interpretation of the NMR chemical shift data

Fig. 6 shows example NMR spectra for pure ethanol and for a mixture of ethanol and CO_2, with x_{EtOH} = 0.095 mol/mol. TMS and acetone are contained in the lock capillary, and hence

neither has an influence on the ethanol system. In the spectrum of the more dilute sample, the TMS and acetone peaks are significantly larger, relatively speaking, than in that of the pure ethanol sample. In the spectrum of pure ethanol, the acetone peak is too small to be seen. As well as the TMS and acetone peaks, both spectra show three clearly defined peaks, corresponding to the CH_3, CH_2 and OH groups. The CH_3 and CH_2 peak shifts as a function of concentration, temperature and pressure are much smaller than that of the OH peak.

As mentioned in the introduction, the change in chemical shift of the CH_2 and CH_3 groups can be attributed to non-hydrogen binding interactions due to changes in the bulk magnetic susceptibility [2] and density effects [37, 38]. These effects are the same for all three proton types (CH_2, CH_3 and OH). Thus, the effect of hydrogen bonding can be isolated for investigation by consideration of the shift of the OH peak, relative to either the CH_2 or CH_3 peak. The relative shift of the CH_n peak (δ_{CHn}) is given by the difference in absolute chemical shifts of the OH (δ(OH)) and the CH_n ($\delta(CH_n)$) peak ($\delta_{CHn} = \delta(OH) - \delta(CH_n)$) [39]. The magnitude of this relative shift is a measure of the extent of hydrogen bonding occurring and is the same for both CH_n groups, although obviously the absolute values for the two peaks are different by several ppm as the two groups are chemically non-equivalent. For details, see Section 5.1.

The distribution of hydrogen bonded species from molecular simulation can be correlated to the experimentally determined relative chemical shift of the OH peak by [8]:

$$\delta = f_0\delta_M + \frac{f_1}{2}\delta_A + \left(\frac{f_1}{2} + f_2 + f_3\right)\delta_D, \quad (4)$$

where δ_M is the relative chemical shift of the monomers, δ_A and δ_D the relative chemical shifts of the ethanol molecules acting as proton acceptor and donor, respectively.

As in our previous study on the methanol system [8], it can be assumed that for molecules acting as both proton donors and acceptors (see Fig. 5 (d)), the de-shielding of the hydroxyl group is primarily determined by proton donation and accordingly these molecules are assigned to δ_D only. Likewise, it was found in the present molecular simulations that the configuration in which the central molecule acts as proton acceptor twice (see. Fig. 5 (e)) practically does not occur. Hence, all species in f_2 exhibit the chemical shift δ_D and the corresponding contribution is $f_2\delta_D$.

As no structural data were used in the model development, the hydrogen bonding statistics from molecular simulations presented in this work are purely predictions.

5. Results and Discussion

5.1. Experimental NMR results

Experimental data for the solution density and the chemical shifts of all three groups at the four examined temperatures and pressures between approximately 5 and 25 MPa, for ethanol concentrations within x_{EtOH} = 0.017 – 1.0 mol/mol are given in the supplementary material. The pressure dependence of the results is so small that it is of the same order of magnitude as the data scatter and hence cannot be quantified reliably (see section 5.2.2). Nevertheless, the relative chemical shifts δ_{CH2} and δ_{CH3} observed at constant concentration and temperature as a function of pressure were fitted to parabolic or linear functions of the pressure as appropriate, and interpolated to 15 MPa to obtain isobaric data. Values interpolated to 15 MPa for δ_{CH2} and δ_{CH3} are given in Table 2.

As previously reported for the methanol system [7], at constant temperature and pressure, the relative shifts can be fitted to a simple analytic function:

$$\delta = a\frac{1+bx_{\mathrm{EtOH}}}{1+cx_{\mathrm{EtOH}}}, \qquad (5)$$

where *a*, *b* and *c* are adjustable parameters. This function is not based on any chemical or physical properties but can be used to extrapolate the relative chemical shifts to infinite dilution. The relative shifts in the absence of any hydrogen bonding are given by the parameter *a*. This value corresponds to the chemical shift of the ethanol monomer, and is later referred to as δ_M. The relative chemical shifts calculated here are in good agreement with previous experimental determinations of the chemical shifts of ethanol in infinitely dilute solutions of CO_2 and CCl_4 (see Table 3).

In Fig. 7, δ_{CH2} and δ_{CH3} are plotted as a function of the logarithmic ethanol concentration for the four temperatures investigated here (top to bottom: 293.15, 308.15, 323.15, 338.15 K). The markers represent measured points; circles for δ_{CH2} and triangles for δ_{CH3}. The dashed and solid lines represent the fits to eq. 5 for δ_{CH2} and δ_{CH3}, respectively. As can be seen from Fig. 7, the results obtained using δ_{CH3} and those obtained using δ_{CH2} are in excellent agreement. As previously seen for methanol [7, 8], the temperature has a significant effect on the degree of hydrogen bonding present in the system. At low temperatures, the relative shifts are significantly larger than at high temperatures, indicating that more hydrogen bonding occurs at low temperatures.

5.2. Molecular simulation results

5.2.1. Temperature and concentration dependence at constant pressure

The dependence of the calculated species fractions, f_i, on temperature and ethanol mole fraction at 15 MPa is shown in Fig. 8. As expected, at lower temperatures and higher ethanol mole fractions (i.e. higher densities of ethanol molecules), increased formation of linear or cross-linked hydrogen bonded chains and tetramers is observed. Thus the fraction, $f_{0,}$ of

ethanol monomers increases with increasing temperature and decreasing ethanol mole fraction (i.e. decreasing density of ethanol molecules results in increasing amounts of monomer species).

The species fraction f_1 (containing one hydrogen bond per molecule) passes through a maximum at ethanol mole fractions between x_{EtOH} = 0.1 and 0.2 mol/mol. The fraction present as this species also increases with increasing temperature. Not surprisingly, the species fractions f_2 and f_3 decrease with decreasing ethanol mole fraction and increasing temperature. This is attributable to the fact that increased mobility at high temperatures hinders the formation of hydrogen bonded chains or tetramers. That f_3 (molecules forming 3 hydrogen bonds) is relatively small indicates that there are few tetramers and cross-linked chain species. As with the experimental results, these species distributions are very similar to the distribution of methanol species published by Schnabel et al. [8].

5.2.2. Temperature and pressure dependence at constant concentration

Fig. 9 shows the dependence of the calculated species fraction on the temperature and pressure at x_{EtOH} = 0.0955 mol/mol. With increasing pressure and hence shorter average distances between the ethanol molecules (higher density of the system) the formation of hydrogen bonded structures such as chains and tetramers is preferred. Hence a decline of the species fraction f_0 (ethanol monomers) with increasing pressure is observed. In contrast, the species fraction of ethanol dimers f_1 is independent of the pressure. As expected, the fraction of ethanol molecules in chains f_2 as well as the fraction of tetramers and cross-linked chain species f_3 increases with increasing pressure. It is obvious that the influence of the pressure on the fractions f_0, f_1 and f_2 is negligible in comparison to the temperature dependence. Only the species fraction f_3 is considerably influenced by the pressure and hence by the density of the system. Nevertheless, this species fraction is very small over the entire pressure range. A

similar influence of pressure on the hydrogen bonding in ethanol was observed by Dellis et al. [35] as well as by Zhang et al. [36] in molecular simulation studies over a wide range of pressures and temperatures. In contrast, in a molecular simulation study of the CO_2-ethanol system, Xu et al. [12] observed a decreasing number of hydrogen bonds between ethanol molecules with increasing pressure. It must be taken into account that these authors also considered the formation of CO_2-ethanol hydrogen bonds which compete with the formation of ethanol-ethanol hydrogen bonds. As the average distance between ethanol and CO_2 molecules decreases with increasing density, the formation of CO_2-ethanol hydrogen bonds increases with increasing pressure [12]. However, according to other reports [13-15], the CO_2-ethanol hydrogen bonds are limited both in number and lifetime and hence were neglected in our study. The dependence of the species fractions f_i on the temperature is described in 5.2.1.

5.3. Comparison of molecular simulation results with NMR data

As stated in Section 3.1, the chemical shift of the monomer δ_M could be directly determined from extrapolation to infinite dilution of the experimental NMR results (see Tables 2 and 3) and is thus independent of the simulation data. The state independent parameters δ_A and δ_D, both relative to CH_2 and CH_3, were fitted with eq. 4 to the experimental data at 15 MPa on the basis of the distribution of hydrogen bonded ethanol species f_i from molecular simulations at 15 MPa. The results are given in Table 4. The value for δ_M given here is an average of the values given in Table 2.

5.3.1. Temperature and concentration dependence at constant pressure

Fig. 10 shows the experimental NMR data (hollow markers) and the calculated fit (lines) to the data based on the simple analytic function shown in eq. 5. Also shown are the fitted chemical shifts based on the simulated species distributions and eq. 4 (filled markers). The

experimental values of δ_{CH2} and δ_{CH3} are well described with respect to the effects of both temperature and ethanol mole fraction. Given the simplicity of the modeling approach compared to the complexity of the physico-chemical phenomena investigated, the deviations are small, even at high temperatures. The predictions of the chemical shifts for ethanol mole fractions of x_{EtOH} = 0.1, 0.2, 0.4, 0.6 and 0.8 mol/mol, as determined from the molecular simulation, are also in good agreement with the experimentally determined fit.

5.3.2. Temperature and pressure dependence at constant concentration

In Fig. 11 the dependence of the calculated chemical shift (filled markers) on the pressure is shown for the temperatures investigated herein. The chemical shifts were determined using eq 4. with the shift parameters δ_M, δ_A and δ_D (Table 4) and the simulated species distributions at x_{EtOH} = 0.0955 mol/mol. The experimental data (hollow markers) for the same concentration, pressures and temperatures are also shown. As expected, the chemical shifts, δ_{CH2} and δ_{CH3}, calculated on the basis of the simulated species distributions increase slightly with increasing pressure (higher density of the system). However, the dependence of the chemical shift on pressure is, in the pressure range of this study, negligible in comparison with the dependence on temperature. Likewise, in the NMR measurements, the influence of pressure, and hence of the density, on the chemical shift is too small to be detected. Thus, it is reasonable to neglect the influence of pressure on the chemical shift for the fit in eq. 5.

5.4. Application of simulation results to the SAFT equation of state

The SAFT (statistical associating fluid theory) equation of state can be used as an alternative to molecular simulations to describe the thermodynamic properties of a system. In the CO_2-ethanol mixtures described in this work, it can be assumed that short-range anisotropic attractions such as hydrogen bonds only occur between ethanol molecules. However, in order to have a model comparable to that used in this work, the SAFT model of the ethanol

molecule must include three association sites (representing the hydrogen atom and the unbounded electron pair on the oxygen site [40]). The association term of the Helmholtz energy can be calculated according to Wertheim`s theory [40] for both pure ethanol and the ethanol + CO_2 mixture. Based on the species distributions calculated in this work, the two adjustable parameters of the association site-site interaction of the SAFT equation [40] can be determined. In this way, these two parameters do not need to be fitted to further experimental data such as vapour pressure and saturated density [40]. It was not in the scope of the present work to carry out this work on SAFT modeling.

6. Conclusions

The simple molecular force field model of the type LJ plus point charges previously developed by our group was used to describe hydrogen bonding within CO_2-ethanol mixtures. An extensive experimental study of the effect of temperature, pressure and concentration on the chemical shifts served to illustrate the validity and accuracy of the model. The system was described in terms of a simple approach including only ethanol monomers, and proton donors or acceptors. Based on this approach, two state-independent parameters for the relative chemical shifts of the donors and acceptors were fitted to the experimental data, speciation profiles and the parameter for the relative chemical shift of the monomer (extrapolated from experimental results). The good agreement between simulated and experimental results demonstrates the validity of the simple molecular model for the ethanol system and indicates that using electrostatic sites for modeling not only polarity but also hydrogen bonds is reasonable.

Acknowledgment

The authors gratefully acknowledge financial support from the Deutsche Forschungsgemeinschaft (DFG) under the grant Ha 1993/ 9-2. We thank Jadran Vrabec from

the University of Paderborn for advice regarding the simulation code. This work was conducted under the auspices of the Boltzmann-Zuse Society of Computational Molecular Engineering (BZS).

Supplementary material available:

The raw chemical shift data of the OH, CH_2 and CH_3 groups for all conditions measured are available in the supplementary material.

7. References

[1] S.J. Grabowski, Hydrogen Bonding - New Insights, Springer, Dordrecht, The Netherlands, 2006.
[2] M.M. Hoffmann, M.S. Conradi, Are there hydrogen bonds in supercritical methanol and ethanol?, Journal of Physical Chemistry B, 102 (1998) 263-271.
[3] S. Bai, C.R. Yonker, Pressure and temperature effects on the hydrogen-bond structures of liquid and supercritical fluid methanol, Journal of Physical Chemistry A, 102 (1998) 8641-8647.
[4] T. Gross, L.P. Chen, J. Buchhauser, H.D. Ludemann, T, P dependence of intradiffusion in binary fluid mixtures with carbon dioxide as one component, Physical Chemistry Chemical Physics, 3 (2001) 2845-2851.
[5] N. Asahi, Y. Nakamura, Nuclear magnetic resonance and molecular dynamics study of methanol up to the supercritical region, Journal of Chemical Physics, 109 (1998) 9879-9887.
[6] T. Tsukahara, M. Harada, H. Tomiyasu, Y. Ikeda, NMR studies on effects of temperature, pressure, and fluorination on structures and dynamics of alcohols in liquid and supercritical states, Journal of Physical Chemistry A, 112 (2008) 9657-9664.
[7] M. Maiwald, H. Li, T. Schnabel, K. Braun, H. Hasse, On-line ^{1}H NMR spectroscopic investigation of hydrogen bonding in supercritical and near critical CO_2-methanol up to 35 MPa and 403 K, Journal of Supercritical Fluids, 43 (2007) 267-275.
[8] T. Schnabel, A. Srivastava, J. Vrabec, H. Hasse, Hydrogen bonding of methanol in supercritical CO_2: comparison between ^{1}H NMR spectroscopic data and molecular simulation results, Journal of Physical Chemistry B, 111 (2007) 9871-9878.
[9] J. Vrabec, J. Stoll, H. Hasse, A set of molecular models for symmetric quadrupolar fluids, Journal of Physical Chemistry B, 105 (2001) 12126-12133.
[10] T. Schnabel, 2008. Molecular modelling and simulation of hydrogen bonding pure fluids and mixtures. Thesis, (PhD) University of Stuttgart.
[11] W.H. Xu, J.C. Yang, A computer simulation study on self- and cross-aggregation of multiple polar species in supercritical carbon dioxide, Journal of Physical Chemistry A, 114 (2010) 5414-5428.
[12] W.H. Xu, J.C. Yang, Y.Y. Hu, Microscopic structure and interaction analysis for supercritical carbon dioxide-ethanol mixtures: a monte carlo simulation study, Journal of Physical Chemistry B, 113 (2009) 4781-4789.

[13] I. Skarmoutsos, E. Guardia, Local structural effects and related dynamics in supercritical ethanol. 2. Hydrogen-bonding network and its effect on single reorientational dynamics, Journal of Physical Chemistry B, 113 (2009) 8898-8910.
[14] I. Skarmoutsos, E. Guardia, J. Samios, Hydrogen bond, electron donor-acceptor dimer, and residence dynamics in supercritical CO_2-ethanol mixtures and the effect of hydrogen bonding on single reorientational and translational dynamics: A molecular dynamics simulation study, Journal of Chemical Physics, 133 (2010) 014504.
[15] M. Saharay, S. Balasubramanian, Electron donor-acceptor interactions in ethanol-CO_2 mixtures: an ab initio molecular dynamics study of supercritical carbon dioxide, Journal of Physical Chemistry B, 110 (2006) 3782-3790.
[16] H. Friebolin, G. Schilling, L. Pohl, New method for determining the temperature in nuclear magnetic resonance spectrometers, Organic Magnetic Resonance, 12 (1979) 569-573.
[17] T. Schnabel, J. Vrabec, H. Hasse, Henry's law constants of methane, nitrogen, oxygen and carbon dioxide in ethanol from 273 to 498 K: Prediction from molecular simulation (vol 233, pg 134, 2005), Fluid Phase Equilibria, 236 (2005) 272.
[18] H.A. Lorentz, Über die anwendung des satzes vom virial in der kinetischen theorie der gase, Annalen der Physik, 12 (1881) 127-136, addendum 660-661.
[19] D. Berthelot, Sur le mélange des gaz, Comptes Rendus Hebdomadaires des Séances de l'Académie des Sciences, 126 (1898) 1703-1706, addendum 1857-1858.
[20] T. Schnabel, J. Vrabec, H. Hasse, Henry's law constants of methane, nitrogen, oxygen and carbon dioxide in ethanol from 273 to 498 K: Prediction from molecular simulation (vol 233, pg 134, 2005), Fluid Phase Equilibria, 239 (2006) 125-126.
[21] J.S. Lim, Y.Y. Lee, H.S. Chun, Phase equilibria for carbon dioxide ethanol water system at elevated pressures. , Journal of Supercritical Fluids, 7 (1994) 219-230.
[22] H. Pöhler, E. Kiran, Volumetric properties of carbon dioxide plus ethanol at high pressures, Journal of Chemical and Engineering Data, 42 (1997) 384-388.
[23] A. Zuniga-Moreno, L.A. Galicia-Luna, Compressed liquid densities of carbon dioxide plus ethanol mixtures at four compositions via a vibrating tube densimeter up to 363 K and 25 MPa, Journal of Chemical and Engineering Data, 47 (2002) 149-154.
[24] E.W. Lemmon, M.O. McLinden, M.L. Huber, NIST reference fluid thermodynamic and transport properties—REFPROP, 2002.
[25] L. Verlet, Computer experiments on classical fluids. I. Thermodynamical properties of Lennard-Jones molecules., Physical Review, 159 (1967) 98-103.
[26] B. Quentrec, C. Brot, New method for searching for neighbours in molecular dynamics computations, Journal of Computational Physics, 13 (1973) 430-432.
[27] R.W. Hockney, J.W. Eastwood, Computer Simulations Using Particles, McGraw Hill, New York, 1981.
[28] M.P. Allen, D.J. Tildesley, Computer Simulation of Liquids, Clarendon Press, Oxford, U.K., 2007.
[29] L. Saiz, J.A. Padró, E. Guàrdia, Structure and dynamics of liquid ethanol, Journal of Physical Chemistry B, 101 (1997) 78-86.
[30] J.A. Padró, L. Saiz, E. Guàrdia, Hydrogen bonding in liquid alcohols: a computer simulation study, Journal of Molecular Structure, 416 (1997) 243-248.
[31] M. Haughney, M. Ferrario, I.R. McDonald, Molecular dynamics simulation of liquid methanol, Journal of Physical Chemistry, 91 (1987) 4934-4940.
[32] I.Y. Shilov, B.M. Rode, V.A. Durov, Long range order and hydrogen bonding in liquid methanol: A Monte Carlo simulation, Chemical Physics, 241 (1999) 75-82.
[33] M. Chalaris, J. Samios, Hydrogen bonding in supercritical methanol. A molecular dynamics investigation, Journal of Physical Chemistry B, 103 (1999) 1161-1166.

[34] E. Guàrdia, J. Martí, J.A. Padró, L. Saiz, A.V. Komolkin, Dynamics in hydrogen bonded liquids: water and alcohols, Journal of Molecular Liquids, 96-7 (2002) 3-17.
[35] D. Dellis, M. Chalaris, J. Samios, Pressure and temperature dependence of the hydrogen bonding in supercritical ethanol: A computer simulation study, Journal of Physical Chemistry B, 109 (2005) 18575-18590.
[36] Y. Zhang, J.C. Yang, Y.X. Yu, Y.G. Li, Structural and hydrogen bond analysis for supercritical ethanol: A molecular simulation study, Journal of Supercritical Fluids, 36 (2005) 145-153.
[37] S.L. Wallen, B.J. Palmer, B.C. Garrett, C.R. Yonker, Density and temperature effects on the hydrogen bond structure of liquid methanol, Journal of Physical Chemistry, 100 (1996) 3959-3964.
[38] S.L. Wallen, B.J. Palmer, B.C. Garrett, C.R. Yonker, Density and temperature effects on the hydrogen bond structure of liquid methanol (vol 100, pg 3959, 1996), Journal of Physical Chemistry, 100 (1996) 20173-20173.
[39] C.R. Yonker, J.C. Linehan, The use of supercritical fluids as solvents for NMR spectroscopy, Progress in Nuclear Magnetic Resonance Spectroscopy, 47 (2005) 95-109.
[40] T. Kraska, K.E. Gubbins, Phase equilibria calculations with a modified SAFT equation of state. 1. Pure alkanes, alkanols, and water, Industrial & Engineering Chemistry Research, 35 (1996) 4727-4737.

Fig. 1

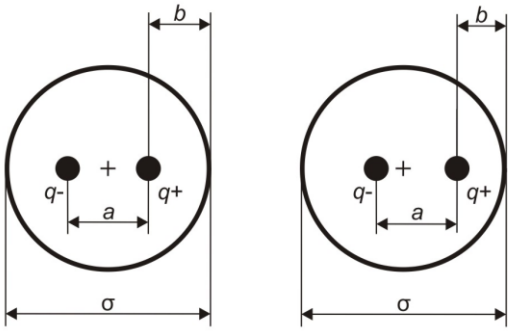

Fig. 2

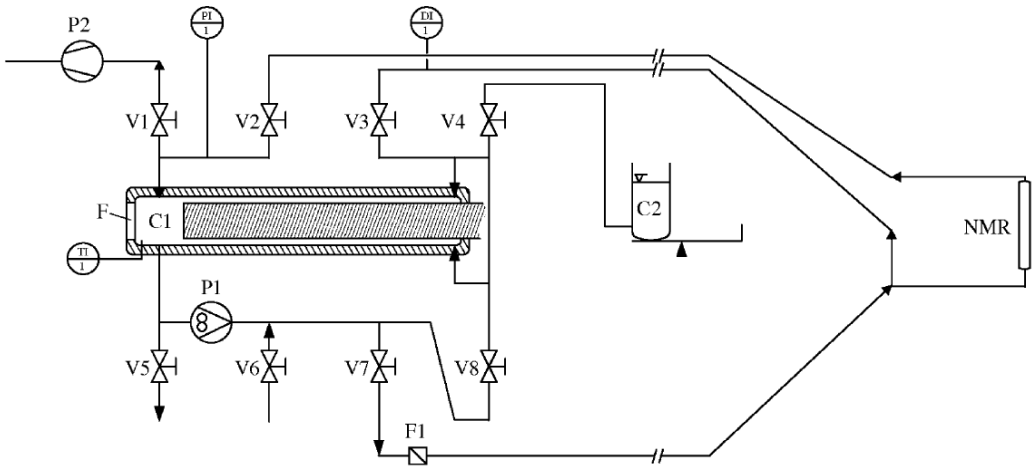

Fig. 3

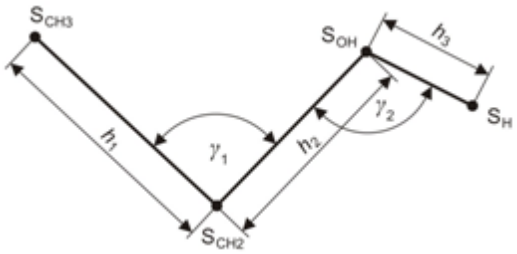

Fig. 4

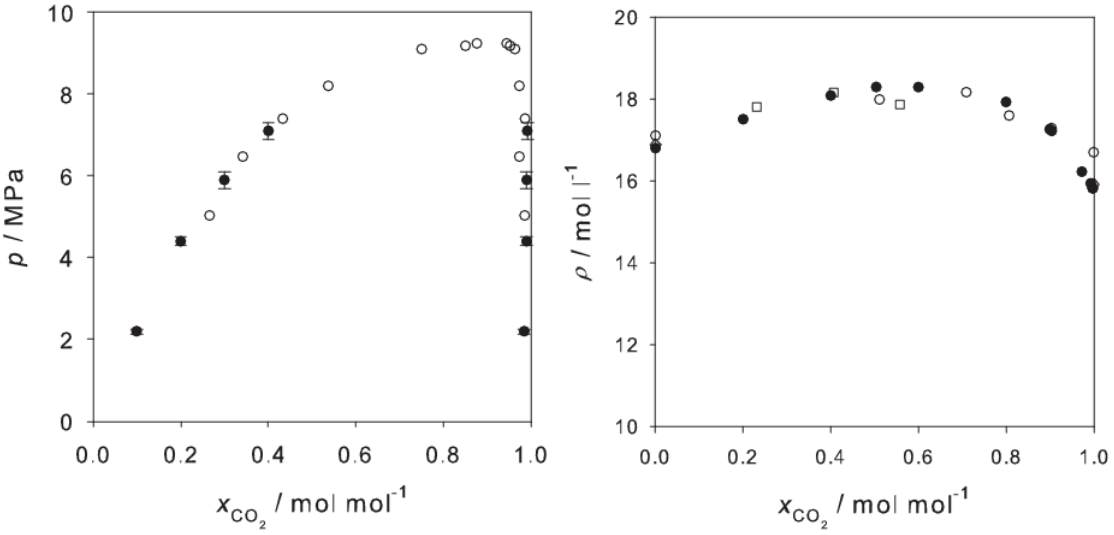

Fig. 5

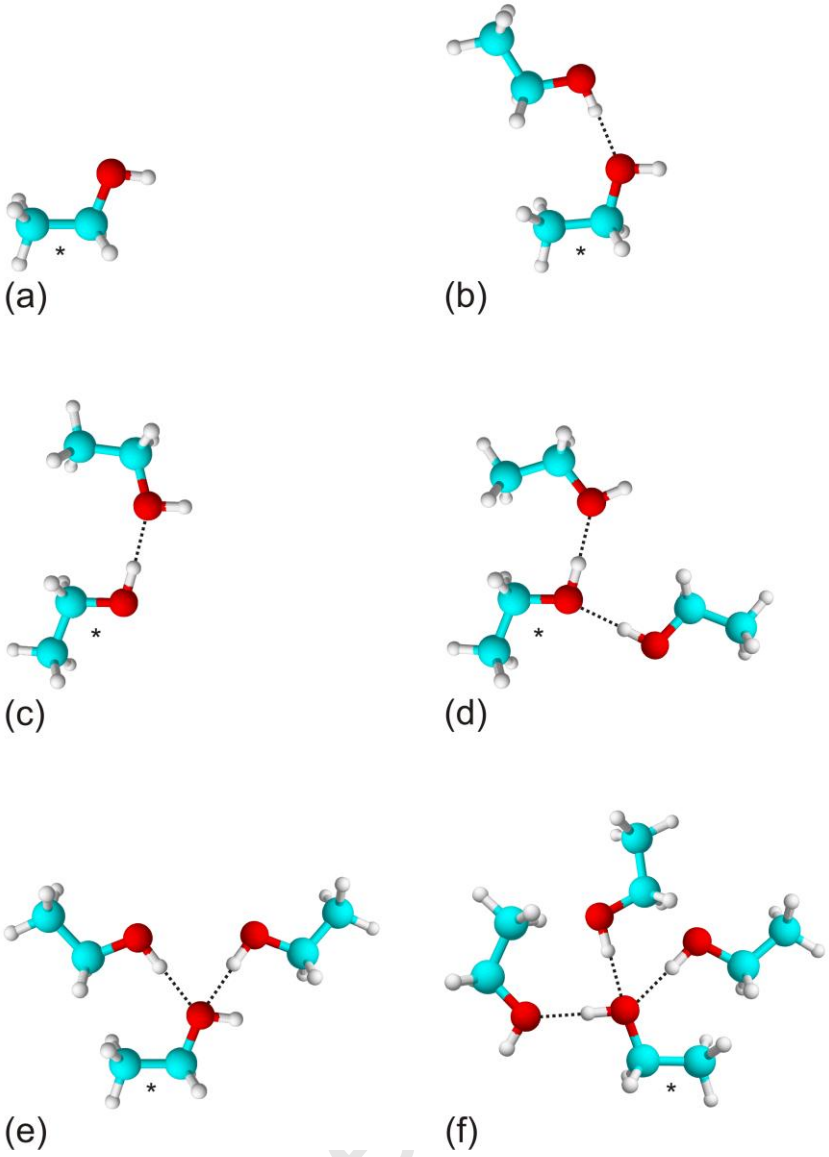

Fig. 6

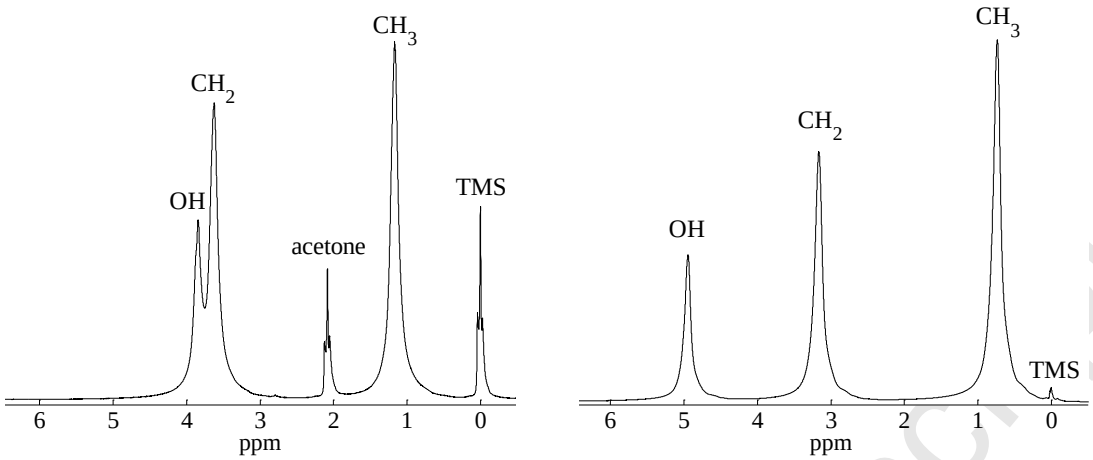

Fig. 7

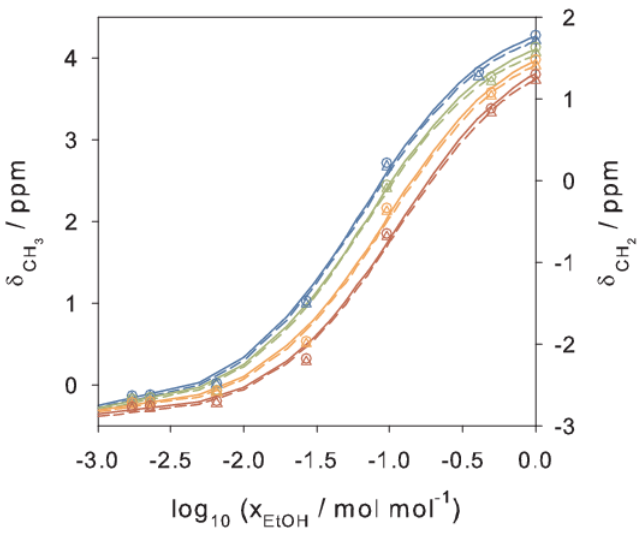

Fig. 8

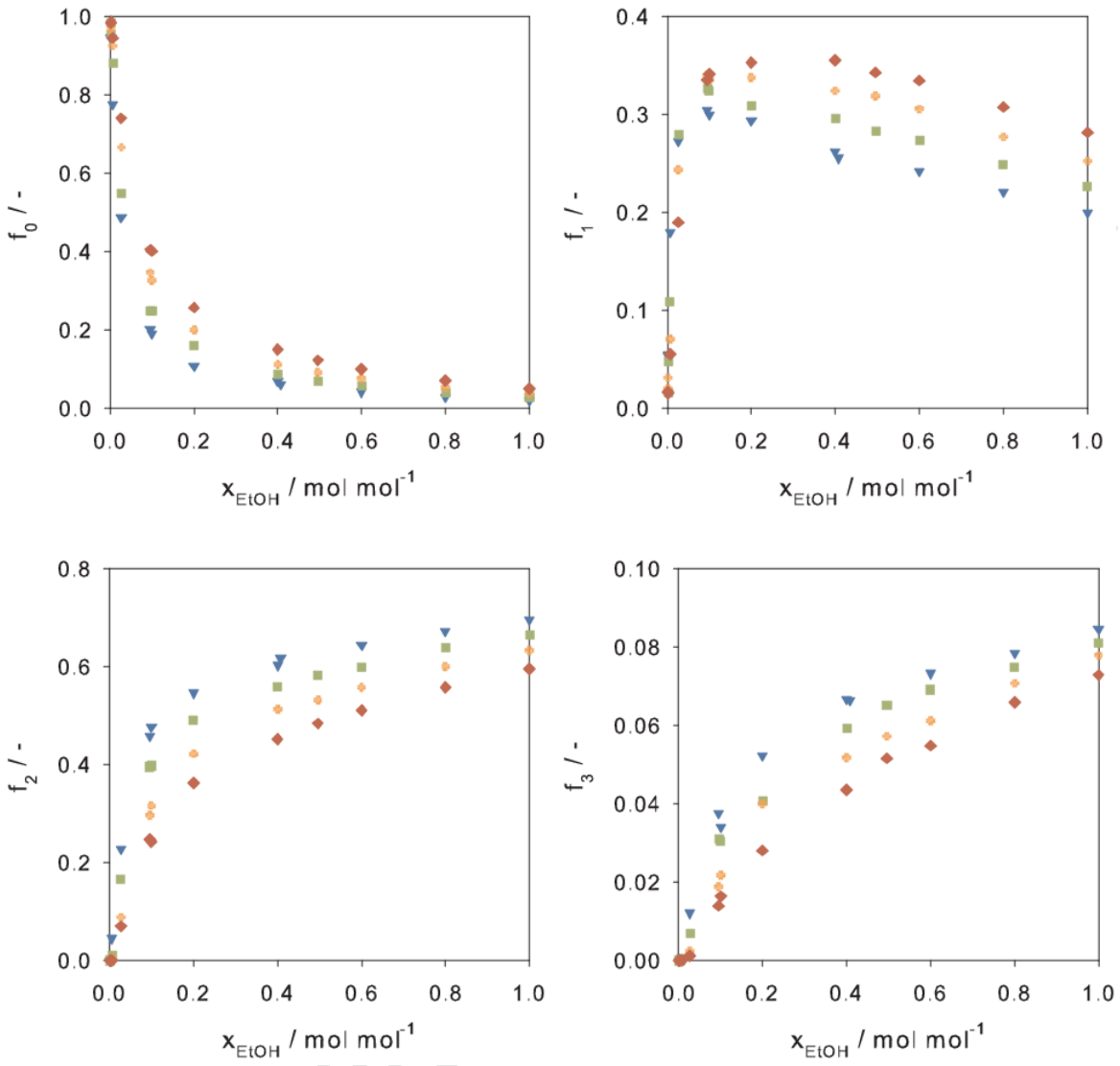

Fig. 9

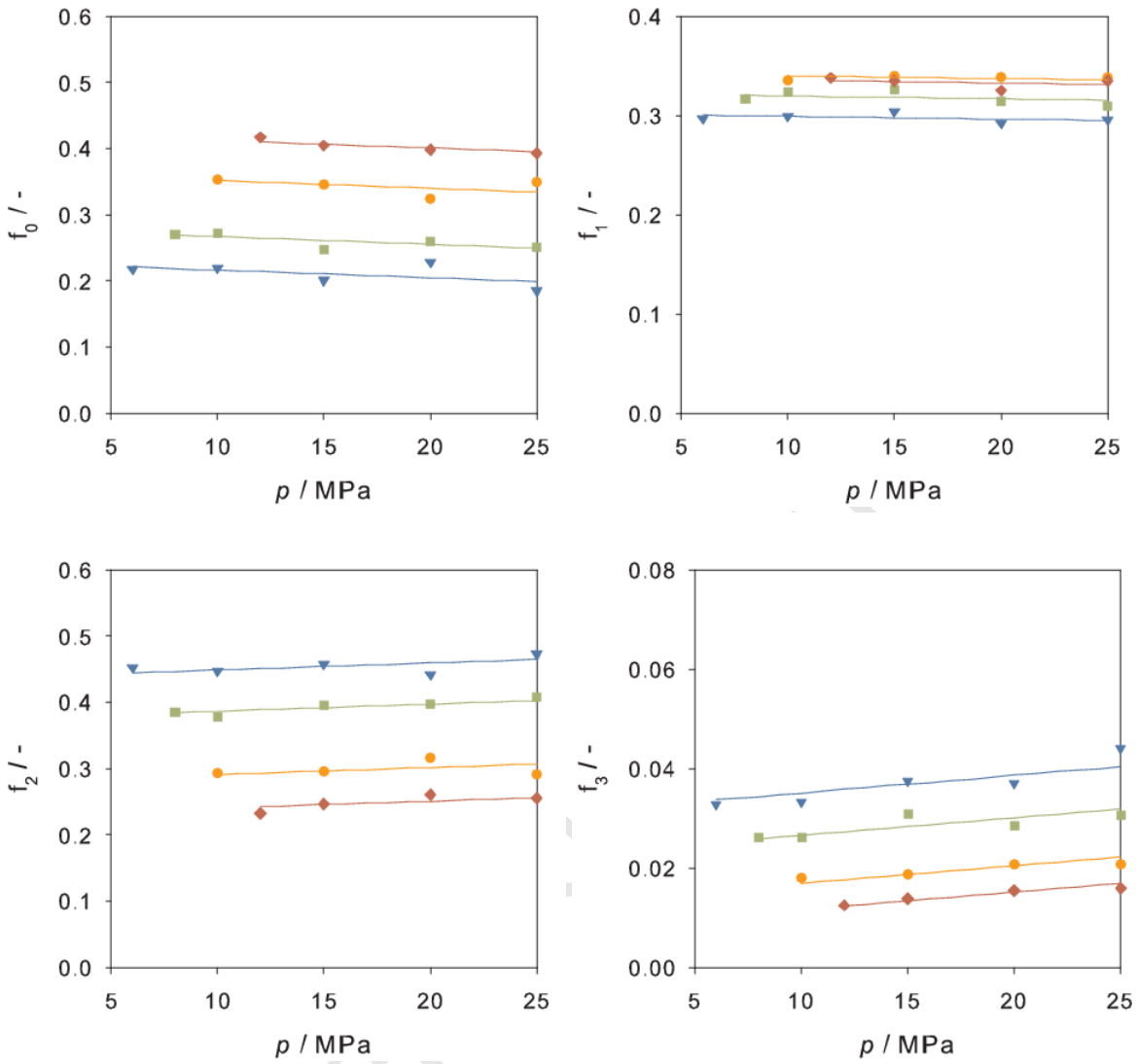

Fig. 10

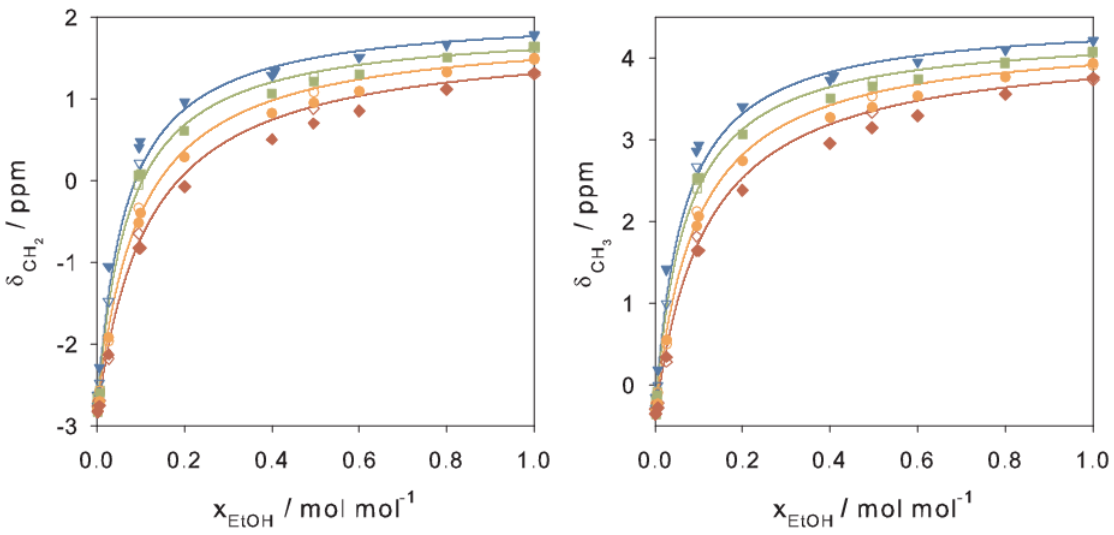

Fig. 11

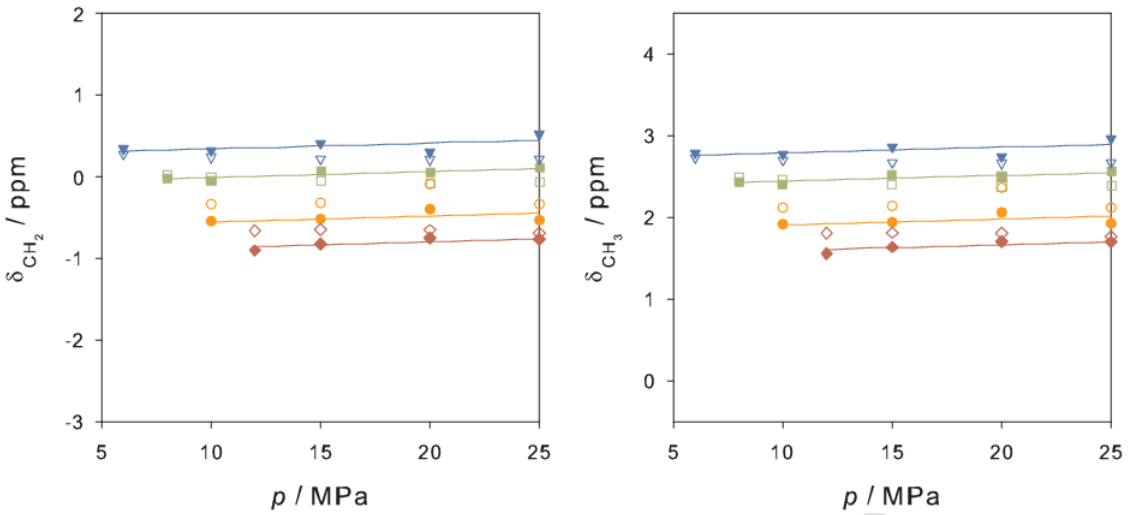

Fig. 5 (black & white)

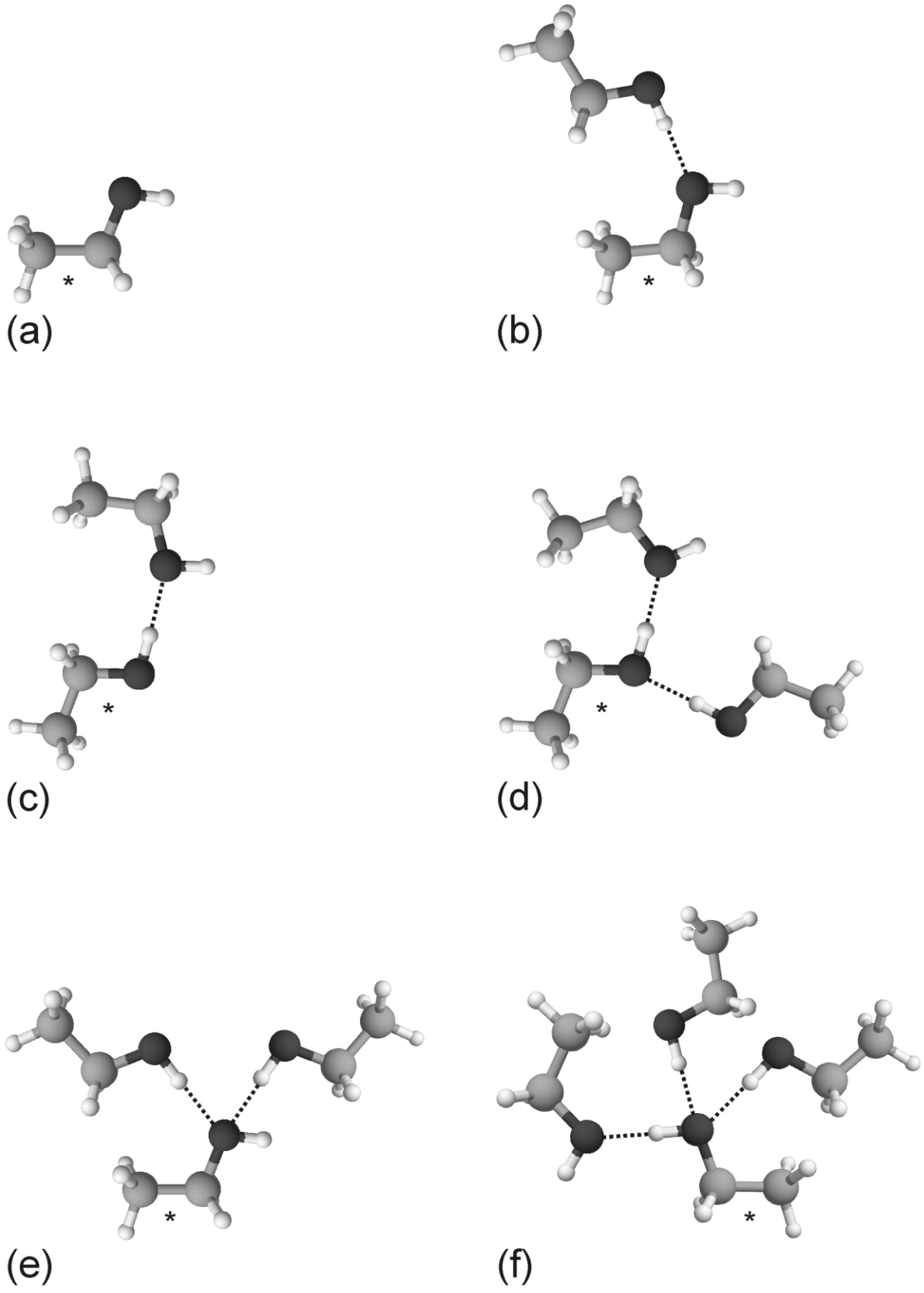

Fig. 7 (black & white)

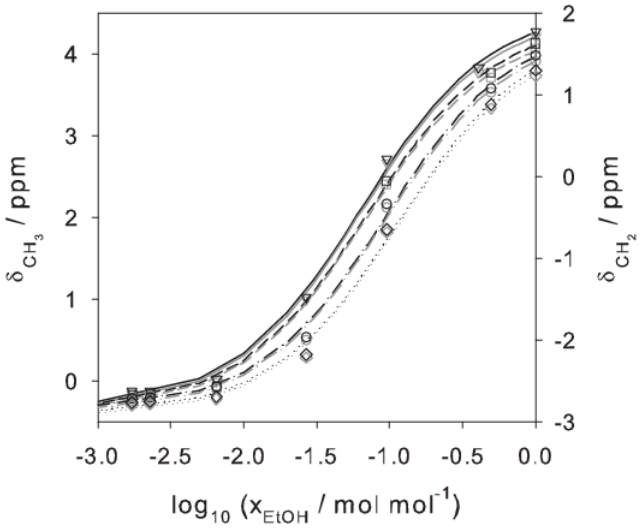

Fig. 8 (black & white)

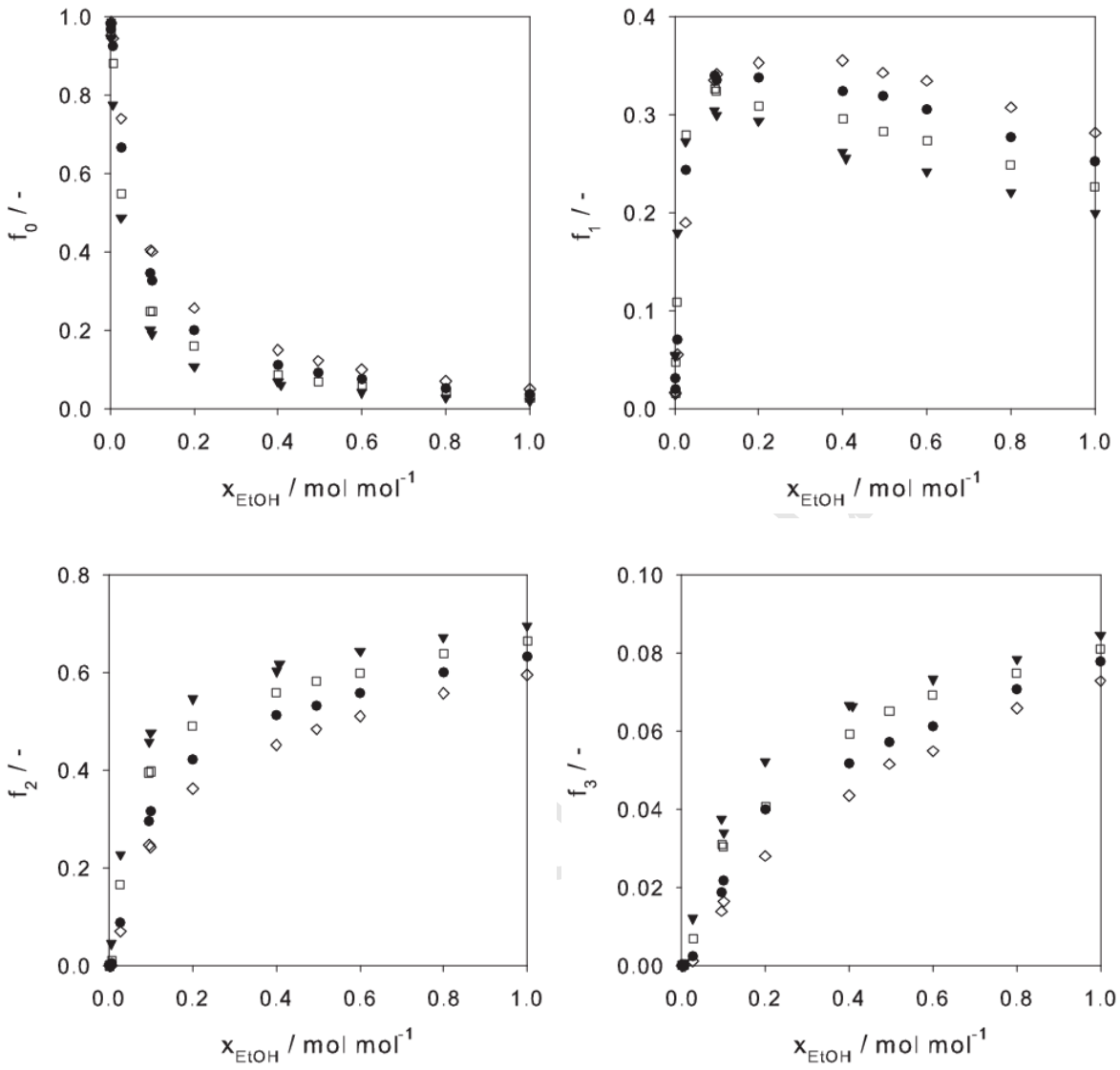

Fig. 9 (black & white)

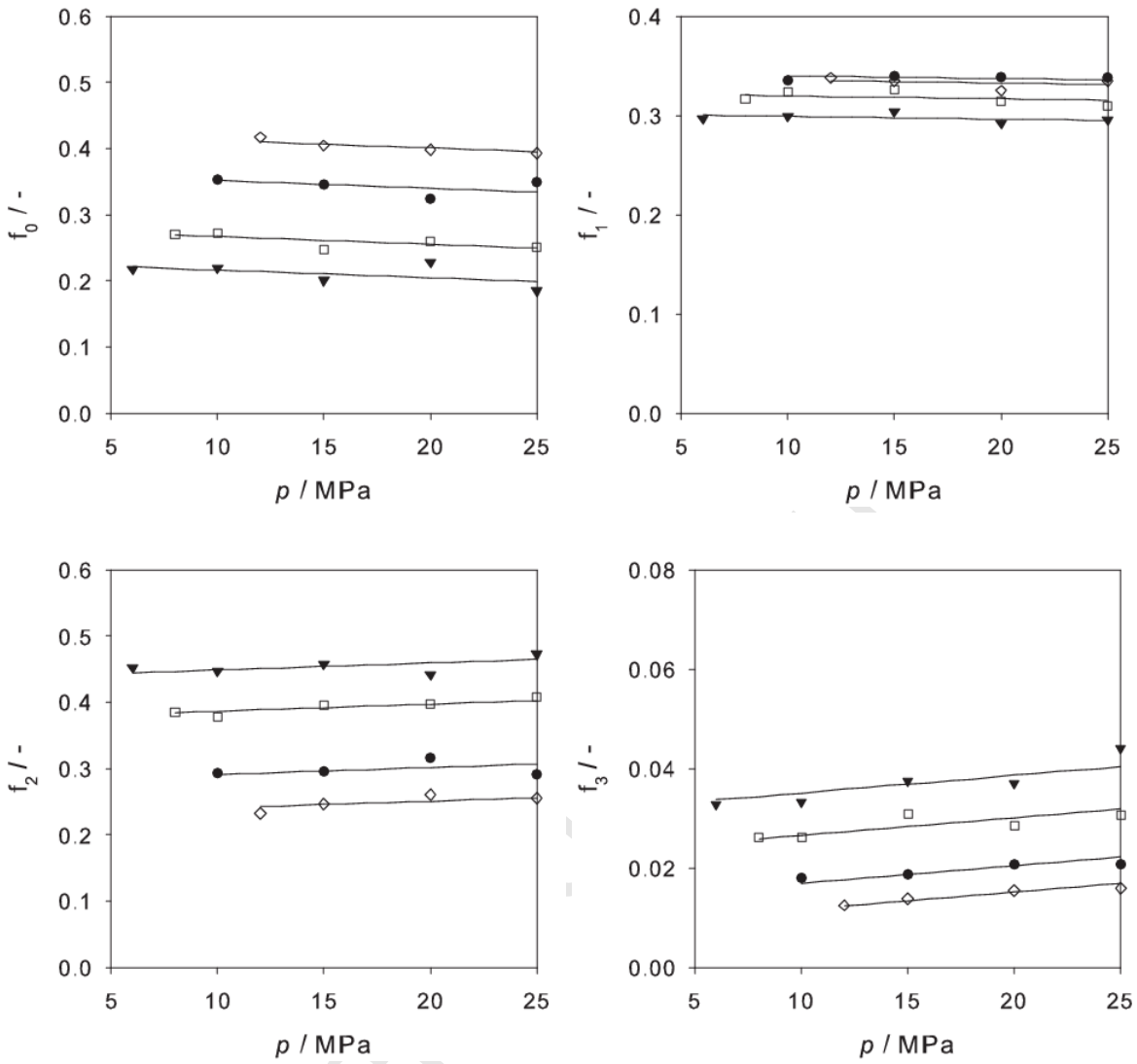

Fig. 10 (black & white)

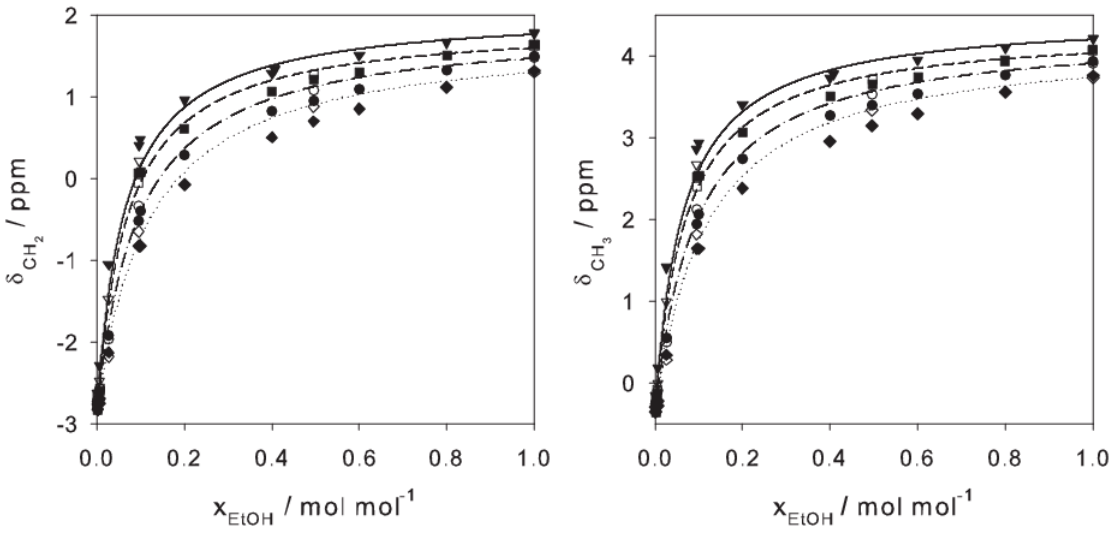

Fig. 11 (black & white)

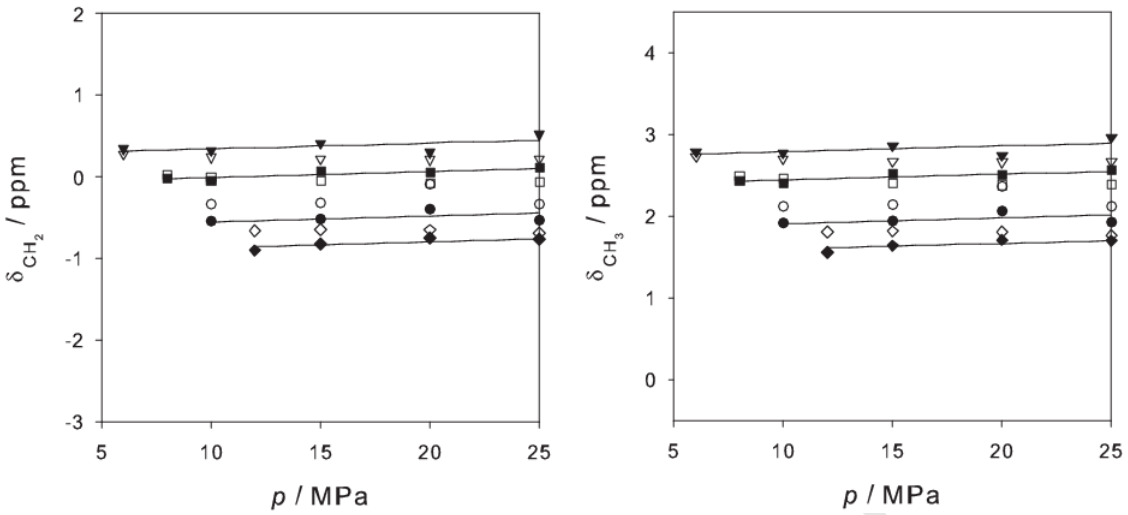

Fig. Captions:

Fig. 1 Molecules composed of one LJ site and two point charges (*q*-, *q*+).

Fig. 2 High pressure on-line NMR set-up: P1 gear pump, P2 vacuum pump, V1 evacuation valve, V2 and V3 NMR return valves, V4 liquid inlet valve, V5 liquid and gas exhaust valve, V6 gas inlet valve, V7 NMR flow valve, V8 high pressure cell recycle valve; C1 sample volume, C2 liquid sample balance, F1 10 μm filter, and D1 vibrating tube densimeter.

Fig. 3 Geometry of the ethanol model: S_i indicates the model interaction site i.

Fig. 4 Left: Vapor-liquid equilibria of ethanol + CO_2: simulation data (filled markers) and experimental data [21] (hollow markers) at 323.15 K. Right: Density of ethanol + CO_2: simulation data (filled markers) and experimental data (hollow markers): ○[22] □[23] ◇[24] at 15 MPa and 323.15 K

Fig. 5 Hydrogen bonded ethanol molecule configurations. The reference molecule is labeled by *; (a) monomer f_0; (b) and (c) dimers, f_1; (d) and (e) central molecule of trimer, f_2; (f) cross-linked central molecule of a tetramer, f_3.

Fig. 6 Example ^{1}H NMR spectra for pure ethanol (right) and x_{EtOH} = 0.095 mol/mol (left) at 293.15 K and 15 MPa.

Fig. 7 Measured results (interpolated to 15 MPa) for δ_{CH2} (right Y-axis, ○) and δ_{CH3} (left Y-axis, △) and results from eq. 5, fitted to each individual series (dashed lines, δ_{CH2}; solid lines, δ_{CH3}). Results at 293.15 K in blue, 308.15 K in green, 323.15 K in orange and 338.15 K in red.

Fig. 8 Species fractions, f_i, from molecular simulations at 15 MPa. The statistical uncertainties are generally within the symbol size. Top left: f_0, top right: f_1, lower left: f_2, lower right f_3. ▼: 293.15 K, ■: 308.15 K, ●: 323.15 K, ◆:338.15 K.

Fig. 9 Species fractions, f_i, from molecular simulations at x_{EtOH} = 0.0955 mol/mol. The statistical uncertainties are generally within the symbol size. Top left: f_0, top right: f_1, lower left: f_2, lower right f_3. ▼: 293.15 K, ■: 308.15 K, ●: 323.15 K, ◆:338.15 K, lines are guides for the eye (linear regression).

Fig. 10 Comparison of experimentally measured chemical shifts (hollow markers) with the fit based on a simple analytic function (solid lines) and the predicted shifts based on simulated speciation profiles and fitted values for δ_A and δ_D (filled markers) at 15 MPa. ▼: 293.15 K, ■: 308.15 K, ●: 323.15 K, ◆:338.15 K. Left: for OH shift relative to CH_2 group, right: for OH shift relative to CH_3 group.

Fig. 11 Comparison of experimentally measured chemical shifts (hollow markers) with the predicted shifts as a function of pressure, based on simulated speciation profiles and fitted values for δ_A and δ_D (filled markers) at 15 MPa. ▼: 293.15 K, ■: 308.15 K, ●: 323.15 K, ◆: 338.15 K, lines are guides for the eye (linear regression) for the simulated shifts. Left: for OH shift relative to CH_2 group, right: for OH shift relative to CH_3 group.

Black and White Fig. Captions: (where not as for coloured Figs.)

Fig. 7 Measured results (markers, interpolated to 15 MPa) for δ_{CH2} (right Y-axis) and δ_{CH3} (left Y-axis) and results from eq. 5, fitted to each individual series (lines). Black markers and

lines: δ_{CH2} , grey, δ_{CH3}, ▽, —: 293.15 K, □,– –: 308.15 K, ○, – • – : 323.15 K, ◇ ,•••:338.15 K.

Fig. 8 Species fractions, f_i, from molecular simulations at 15 MPa. The statistical uncertainties are generally within the symbol size. Top left: f_0, top right: f_1, lower left: f_2, lower right f_3. ▼: 293.15 K, □: 308.15 K, ●: 323.15 K, ◇:338.15 K.

Fig. 9 Species fractions, f_i, from molecular simulations at x_{EtOH} = 0.0955 mol/mol. The statistical uncertainties are generally within the symbol size. Top left: f_0, top right: f_1, lower left: f_2, lower right f_3. ▼: 293.15 K, □: 308.15 K, ●: 323.15 K, ◇: 338.15 K, lines are guides for the eye (linear regression).

Fig.10 Comparison of experimentally measured chemical shifts (hollow markers) with the fit based on a simple analytic function (lines) and the predicted shifts based on simulated speciation profiles and fitted values for δ_A and δ_D (filled markers) at 15 MPa. ▼,—: 293.15 K, ■,– –: 308.15 K, ●, – • – : 323.15 K, ◆,•••:338.15 K. Left: for OH shift relative to CH_2 group, right: for OH shift relative to CH_3 group.

Fig. 11 Comparison of experimentally measured chemical shifts (hollow markers) with the predicted shifts as a function of pressure based on simulated speciation profiles and fitted values for δ_A and δ_D (filled markers) at 15 MPa. ▼: 293.15 K, ■: 308.15 K, ●: 323.15 K, ◆: 338.15 K, lines are guides for the eye (linear regression) for the simulated shifts. Left: for OH shift relative to CH_2 group, right: for OH shift relative to CH_3 group.

Tables

Table 1 LJ, point charge and geometry parameters of the present ethanol model, cf. Figure 3.

site	σ_{aa} /Å	ε_{aa} / k_B /K	q_a /e
S_{CH3}	3.6072	120.15	0
S_{CH2}	3.4612	86.291	0.25560
S_{OH}	3.1496	85.053	-0.69711
S_H	0	0	0.44151

h_1 /Å	h_2 /Å	h_3 /Å	γ_1 /°	γ_2 /°
1.98420	1.71581	0.95053	90.950	106.368

Table 2 Processed data: Relative chemical shifts (δ_{CHn}, ppm) of the OH group. Values have been interpolated to 15 MPa, using a quadratic fit.

T / K	x_{EtOH} mol/mol	1.0000	0.4960*	0.0268	0.0955	0.0065	0.0023	0.0017	a
293.15	δ_{CH2}	1.780	1.329	-1.471	0.217	-2.477	-2.619	-2.630	-2.828
	δ_{CH3}	4.213	3.775	0.992	2.673	0.000	-0.149	-0.159	-0.356
308.15	δ_{CH2}	1.633	1.268		-0.053	-2.563	-2.654	-2.670	-2.845
	δ_{CH3}	4.062	3.711		2.404	-0.086	-0.185	-0.198	-0.373

323.15	δ_{CH2}	1.482	1.080	-1.965	-0.335	-2.571	-2.702	-2.714	-2.853
	δ_{CH3}	3.910	3.530	0.498	2.122	-0.095	-0.232	-0.244	-0.381
338.15	δ_{CH2}	1.301	0.883	-2.176	-0.647	-2.696	-2.752	-2.768	-2.901
	δ_{CH3}	3.731	3.333	0.286	1.817	-0.225	-0.285	-0.294	-0.432

*At 293.15 K, no value for x_{EtOH} = 0.4960 mol/mol was measured, instead the reported value is for x_{EtOH} = 0.4078 mol/mol.

Table 3 Relative chemical shifts of infinitely dilute ethanol.

δ_{M_CH2} / ppm	δ_{M_CH3} / ppm	T / K	p / MPa	solvent	reference
2.828	0.356	293.15	15	CO_2	This work
2.845	0.373	308.15			
2.853	0.381	323.15			
2.901	0.432	338.15			
N/A	0.41	300 ± 3	0.1	CCl_4	[40]
	0.47	295.15	0.1	CCl_4	[41]
2.732	0.261	313.3	20	CO_2	[42]

Table 4 Fitted relative chemical shifts of the different hydrogen bonded species

	δ_M / ppm	δ_A / ppm	δ_D / ppm
CH_2	-2.8568	-4.7265	2.6305
CH_3	-0.3855	-2.1642	5.0464